Switching Frequency Regulation in Sliding Mode Control by a Hysteresis Band Controller

Victor Repecho, Domingo Biel, Josep M. Olm, *Member, IEEE*, and Enric Fossas, *Member, IEEE*

***Abstract*—Fixing the switching frequency is a key issue in sliding mode control implementations. This paper presents a hysteresis band controller capable of setting a constant value for the steady state switching frequency of a sliding mode controller in regulation and tracking tasks. The proposed architecture relies on a piecewise linear modeling of the switching function behavior within the hysteresis band, and consists of a discrete-time integral-type controller that modifies the amplitude of the hysteresis band of the comparator in accordance with the error between the desired and the actually measured switching period. For tracking purposes an additional feedforward action is introduced to compensate the time variation of the switching function derivatives at either sides of the switching hyperplane in the steady state. Stability proofs are provided, and a design criterion for the control parameters to guarantee closed-loop stability is subsequently derived. Numerical simulations and experimental results validate the proposal.**

Keywords*—Sliding mode control, fixed switching frequency, hysteresis band controller.

I. Introduction

Sliding mode control (SMC) constitutes a natural control tool for variable structure systems (VSS), which are nonlinear systems where the control inputs are inherently discontinuous functions of time. SMC is able to provide directly the control signal to the system without requiring any modulation method, as could be a Pulse Width Modulator (PWM). Due to its well known order reduction and robustness features, SMC is a suitable control option for systems with uncertain dynamics and/or vulnerable to disturbances. Besides, sliding mode controllers provide fast transient responses, because of their ability to use all the available system gain.

The natural way to implement a sliding mode controller is a sign function, but the ideally infinite switching frequency required for the sliding mode to exist restricts its use. A realistic approximation was reported in [2], [3], where a hysteresis comparator replaces the sign function, thus enforcing the control action to switch at finite frequency. Although a finite switching frequency is obtained, it is variable and system dependent [4], [5]. In turn, finite switching frequency control actions entail the appearance of chattering: while a bounded chattering could be acceptable for a given system, it becomes a severe drawback in variable switching frequency conditions because its amplitude changes with the switching frequency and the plant parameters.

Thus, switching frequency reduction is a field of active research, and interesting results have been obtained with predictive sliding mode in a unity power factor rectifier [7], and with double hysteresis band schemes in active filters [8] and voltage source inverters [9].

Special attention has to be taken when implementing sliding mode controllers in power converters, where the need to operate at a constant switching fixed frequency is crucial, because these systems are composed by reactive components and their correct sizing strongly depends on the system switching frequency. Interesting implementation issues with fixed hysteresis band were reported in [6] for elementary power converters.

Several methods can be found in the literature to regulate the SMC switching frequency to a fixed value. Some authors propose the use of an adaptive hysteresis band for the comparator, adjusting its value in accordance with the system state [10]–[15]. This method provides good results, but perfect knowledge of the plant is required. A proper adaptation of the hysteresis band amplitude, which in fact depends on the equivalent control values, demands the use of additional sensors and/or observers, thus increasing costs and reducing system reliability.

In [16], [17] the use of an external signal to force a fixed switching frequency in SMC is presented. The proposal requires new hardware on the controller and only works properly when the switching frequency is low enough with respect to the time constants of the system: in fact, when the switching frequency is increased the state dynamics drifts away from the ideal sliding mode, and a steady-state error appears.

A fixed switching frequency can be obtained by means of the Zero Averaged Dynamics (ZAD) method. This concept was presented in [18] and later on implemented in [19]. The main goal of the ZAD strategy consists in computing a duty cycle that guarantees a zero T-periodic mean value of the switching function, with T denoting the switching period. As a consequence, the steady-state switching period is fixed at a desired value and the averaged overall performance is close to the ideal sliding mode one. Complex calculations and fast processing requirements are the main drawbacks of ZAD-based SMC fixed frequency implementations.

The so-called PWM-SMC was proposed in [20], [21]. This method implements directly an ideal equivalent control calculated from a desired switching surface by a PWM at fixed frequency, while an algorithm to estimate the switching

The authors are with the Institute of Industrial and Control Engineering, Universitat Politècnica de Catalunya, 08028 Barcelona, Spain. D. Biel is also with the Department of Electronic Engineering, Universitat Politècnica de Catalunya. E-mails: victor.repecho.del@upc.edu, domingo.biel@upc.edu, josep.olm@upc.edu, enric.fossas@upc.edu.

A preliminary version of this paper was presented at the 13th International Workshop on Variable Structure Systems, see reference [1].

surface parameters was recently proposed in [23]. Results were summarized in [22], confirming an overall good performance. However, this solution can be derived without using sliding mode concepts, as the equivalent control is a continuous-time function that could be extracted imposing a desired dynamics to the system. Furthermore, some key sliding mode properties, as the previously mentioned order reduction and robustness in the face of disturbances, could be lost. SMC desigs with fixed switching frequency also achieved via PWM implementation were introduced in [25] and [26]. In the latter, the control law is smoothed within a boundary layer to reduce chattering effects, at the cost of a performance reduction of the SMC.

The approach presented in this paper stems from the implementation of SMC by means of a hysteresis band comparator, where the switching frequency is fixed at steady state. A similar scheme was proposed for regulation purposes in [24], [27]–[29], where constant switching frequency operation was reached by means of a PI control loop that adjusts the hysteresis amplitude value. The design of the control parameters was made such that the dynamics of the switching frequency loop was slow enough to avoid interactions with the voltage and current loops [24], [27], and ensures local stability of the linearized system around the equilibrium point, [28], [29]. However, the proposal presented here is within an SMC framework, which allows to develop a large signal model and to analyze the frequency control loop. Therefore, the controller design guarantees stability and asymptotic tendency to a constant switching frequency when the system is on the sliding surface. Furthermore, the addition of an appropriate feedforward term to the integral action allows the extension of the technique to tracking tasks, where small signal modelling can no longer be applied.

The article is structured as follows. The mathematical model of the switching frequency is derived in Section II. The control architecture for both regulation and tracking tasks is included in Section III, followed by the corresponding stability analysis in Section IV. Numerical and experimental results are presented in Sections V and VI, respectively. Finally, conclusions are drawn in Section VII.

II. Mathematical model of the switching frequency behavior

Let us consider an affine single-input single-output (SISO) plant with dynamics given by

$$\dot{x} = f(x) + g(x)u, \tag{1}$$

where $x \in \mathbb{R}^n$ denotes the state, $f, g : \mathbb{R}^n \longrightarrow \mathbb{R}^n$ are smooth vector fields, and $u \in \mathbb{R}$ is the control input.

Let also $s : \mathbb{R}^n \times \mathbb{R} \longrightarrow \mathbb{R}$ be a smooth scalar function and consider the set

$$S := \{x \in \mathbb{R}^n; \quad s(x,t) = 0\}.$$

We refer to $s = s(x,t)$ as the switching function, while S stands for the switching surface.

Assume that the hysteretic control law

$$u = \begin{cases} u^+ & \text{if} \quad s < -\Delta, \\ u^- & \text{if} \quad s > \Delta, \end{cases} \tag{2}$$

where Δ is the hysteresis band width, $\Delta > 0$, and $u^{\pm} := \{u^+, u^-\} \in \mathbb{R}$ denote constant control gains with $u^+ > u^-$, is able to maintain the system within the boundary layer $|s(x,t)| \leq \Delta$, from a certain finite time instant.

Finally, let Δ be small enough and such that $\Delta \to 0$ yields $s \to 0$: hence, an ideal sliding motion is enforced on S. The equivalent control, u_{eq}, that ideally keeps the system sliding on S may be found imposing that S be an invariant manifold for system (1), namely, working out $s(x,t) = 0$, $\dot{s}(x,t,u_{eq}) = 0$, with

$$\dot{s}(x,t,u) = \frac{\partial s}{\partial x} f(x) + \frac{\partial s}{\partial x} g(x) u + \frac{\partial s}{\partial t}. \tag{3}$$

It is therefore immediate that

$$u_{eq} := u_{eq}(x,t) = -\left(\frac{\partial s}{\partial x} g(x)\right)^{-1} \left(\frac{\partial s}{\partial x} f(x) + \frac{\partial s}{\partial t}\right). \tag{4}$$

However, $u = u_{eq}$ cannot be obtained with the realistic, discontinuous control law (2) because of the continuity of u_{eq}. Thus, even though $\Delta \to 0$ may entail $s \to 0$, it does not happen the same with $\dot{s}$ [30]. This may be observed expressing $\dot{s}$ in terms of u_{eq}, replacing u by $u + u_{eq} - u_{eq}$ in (3) and using (4), this yielding

$$\dot{s}(x,t,u) = (u - u_{eq}) \frac{\partial s}{\partial x} g(x). \tag{5}$$

In turn, the control action may be written as

$$u = u_{eq} + \left(\frac{\partial s}{\partial x} g(x)\right)^{-1} \dot{s}$$

and, consequently, the system dynamics within the boundary layer is given by

$$\dot{x} = f(x) + g(x)u_{eq} + g(x)\left(\frac{\partial s}{\partial x} g(x)\right)^{-1} \dot{s}. \tag{6}$$

The third term on the right hand side of (6) is the responsible of the chattering phenomenon observed in realistic sliding regimes [30].

A. Time-invariant hysteresis band amplitude

Assume for the switching function, s, a piecewise linear behavior within the boundary layer, i.e. such that $\dot{s}$ shows piecewise constant values at either side of the switching surface during a complete switching period. This hypothesis makes sense when the switching frequency is high enough with respect to the time constants of the system, and has been often made in the sliding mode control literature (see, for example, [30]).

An expression for $\dot{s}^{\pm}$ follows easily from (5):

$$\dot{s}^{\pm} := \dot{s}(x,t,u^{\pm}) = \left(u^{\pm} - u_{eq}(x,t)\right) \frac{\partial s}{\partial x} g(x). \tag{7}$$

Notice that the assumption of existence of ideal sliding motion ensures $\dot{s}^{\pm} \neq 0$, because it entails the fulfillment of the transversality condition [31]

$$\frac{\partial s}{\partial x} g(x) \neq 0, \tag{8}$$

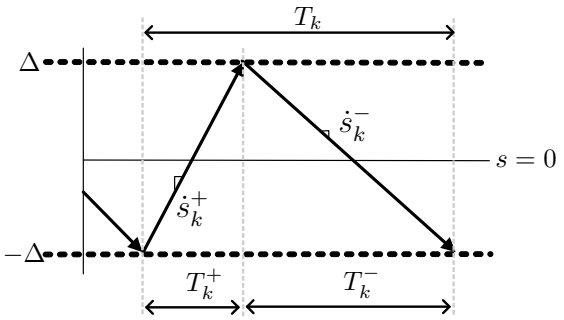

Fig. 1. Switching function behavior in the vicinity of the switching surface, within a constant amplitude boundary layer.

as well as the location of the system within the sliding domain [31], which is the state space region defined by

$$u^- < u_{eq}(x,t) < u^+. \tag{9}$$

Even more, as (2) and (9) reveal an orientation of the switching surface such that (8) is not only non null but positive, it follows immediately that $\dot{s}^+ > 0$ and $\dot{s}^+ < 0$ (see also Figure 1). Hence, defining

$$\rho^\pm := \rho^\pm\left(x,t,u^\pm\right) = \frac{1}{\dot{s}^\pm}, \tag{10}$$

we have that

$$\rho^+ > 0, \quad \rho^- < 0, \quad \forall t \geq 0. \tag{11}$$

Let the system be sampled at every switching period, with $T_k := T(k)$, $k \geq 1$, denoting the k-th switching period, $t_k = \sum_{i=1}^{k} T_k$ indicating the sampling time instants, and $t_0 \geq 0$ being an initial time. Figure 1 shows the behavior of s when evolves from $s = -\Delta$ to $s = \Delta$ and vice-versa within the k-th switching period. The required time to reach $s = \Delta$ from $s = -\Delta$ is denoted with T_k^+ whereas T_k^- is the time needed to recover $s = -\Delta$ from $s = \Delta$. Notice that the dead time used to commute the power switches has been neglected. Hence, in accordance with Figure 1 and (11), the switching period T_k is given by

$$T_k = T_k^+ + T_k^- = 2\Delta\left(\frac{1}{\dot{s}_k^+} - \frac{1}{\dot{s}_k^-}\right) \tag{12}$$

and recalling from (10) that $\rho_k^+ = \frac{1}{\dot{s}_k^+}$ and $\rho_k^- = \frac{1}{\dot{s}_k^-}$, then

$$T_k = T_k^+ + T_k^- = 2\Delta\left(\rho_k^+ - \rho_k^-\right). \tag{13}$$

Notice from (13) that switching period variations observed in generic hysteresis-based sliding mode controlled systems with constant hysteresis band amplitude are actually due to its state and time dependency.

B. Time-varying hysteresis band amplitude

Let us now assume that the hysteresis band amplitude can be modified at the beginning of each switching interval, and that it remains constant up to the next switching interval.

Assuming again piecewise linearity for the scalar function $s = s(x,t,u)$ within the boundary layer, and keeping the notation introduced in Subsection II-A, the behavior of s may be now depicted as in Figure 2. Hence, the k-th switching period is now given by:

$$\begin{aligned} T_k = T_k^+ + T_k^- &= \rho_k^+\left(\Delta_k + \Delta_{k-1}\right) - 2\rho_k^-\Delta_k = \\ &= \hat{\rho}_k\Delta_k + \left(\tilde{\rho}_k - \hat{\rho}_k\right)\Delta_{k-1}, \end{aligned} \tag{14}$$

with

$$\hat{\rho} := \rho^+ - 2\rho^-, \tag{15}$$

$$\tilde{\rho} := 2\left(\rho^+ - \rho^-\right). \tag{16}$$

Let now T^* be a certain switching period reference value, and let us define the switching period error as $e := T^* - T$. Hence, using (14) one easily finds out that

$$\begin{aligned} e_k - e_{k-1} =& \hat{\rho}_k\left(\Delta_{k-1} - \Delta_k\right) + \rho_{k-1}^+\left(\Delta_{k-2} - \Delta_{k-1}\right) + \\ &+ \left(\tilde{\rho}_{k-1} - \tilde{\rho}_k\right)\Delta_{k-1}. \end{aligned} \tag{17}$$

Expression (17) suggests that an appropriately designed control sequence for the hysteresis band amplitude, Δ_k, might yield $e_k \to 0$. Next section is devoted to this purpose.

III. Control architecture for switching frequency regulation

The method proposed below is intended to regulate the switching frequency of the sliding mode controller in the steady state to a reference, constant value T^* using the hysteresis band amplitude of the comparator as the control signal. The appropriate hysteresis value is delivered by a switching frequency controller (SFC), which uses as an input the error between the desired and the actual switching period. The overall controller architecture, including both the switching frequency regulation control loop and the sliding mode control loop, is depicted in Figure 3. The desired steady state ideal sliding dynamics is denoted as $x(t) = x^*(t) \in S$, $\forall t \geq 0$. Hence, $x^* := x^*(t)$ is assumed to be an (asymptotically) stable, positive limit set of (6) with $\dot{s} = 0$, i.e. of

$$\dot{x} = f(x) + g(x)u_{eq}.$$

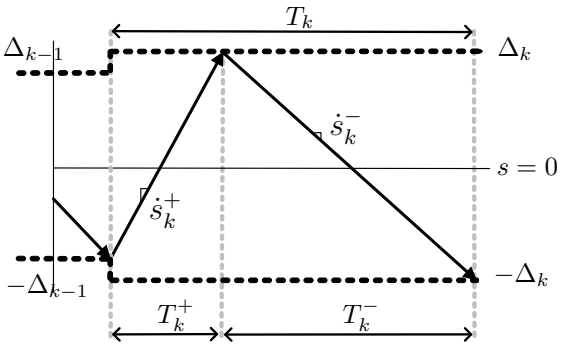

Fig. 2. Switching function behavior in the vicinity of the switching surface, within a time-varying amplitude boundary layer.

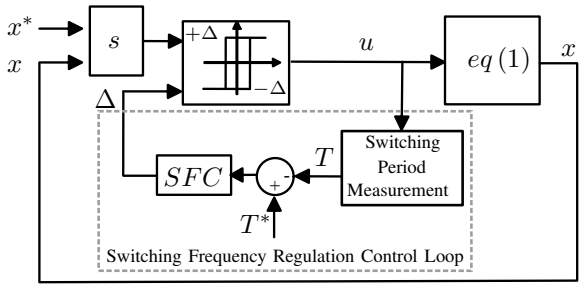

Fig. 3. Overall controller architecture.

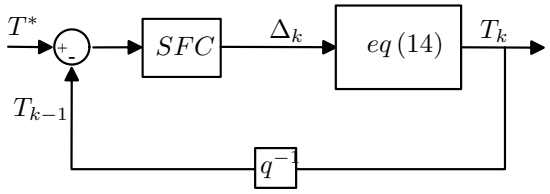

Fig. 4. Detail of the switching frequency regulation control loop.

Figure 4 details the switching frequency control loop. The control scheme operates in asynchronous discrete events given by the switching periods, in accordance with the model developed in Section II. Essentially, the duration of every switching period is measured and compared with the reference value, and this information is used by the SFC to compute a value for the hysteresis band amplitude using an algorithm inspired in (17). Such a control law differs for regulation and tracking tasks, i.e for x^* constant or time-varying, and is specified in next subsections. Finally, the block that provides the hysteresis amplitude as a function of the switching period, modelled by (14), completes the loop. A unit delay, q^{-1}, is included in the feedback path due to the time required to measure the switching period.

Remark 1: Arbitrarily high hysteresis band amplitudes may take the system far away from an ideal sliding regime. Hence, a specific range $\mathcal{I}_\Delta := [\Delta_{min}, \Delta_{max}]$ such that $\Delta_k \in \mathcal{I}_\Delta$, $\forall k \geq 0$, has to be defined so as to preserve the existence of sliding motion. In order to establish the suitable hysteresis range for a given system, the following design criterion is proposed: Δ_{min} may be obtained from the maximum allowable switching frequency, while the maximum acceptable ripple for the state variables would be used to set Δ_{max} and, consequently, the minimum switching frequency. In turn, the switching frequency reference should be accordingly selected within these extremal values.

A. The regulation case

In regulation tasks the state vector reference, x^*, also assumed to be the steady state of the ideal sliding dynamics, is constant. However, in the realistic sliding motion induced by the hysteretic control (2) the state vector chatters within the boundary layer around the state reference. Recalling that, in accordance with Remark 1, the utilized hysteresis band amplitude values keep the state vector ripple low enough, the approximation $x = x^*$ in the steady state is taken as a fact. As the switching hyperplane is now time-invariant, and the corresponding equivalent control (4) is constant in the steady state, the switching function derivatives (7) and its inverses (10) in the steady state are constant as well. Consequently, from a certain discrete-time instant k_0 it results that

$$\rho_k^\pm = \rho\left(x^*, u^\pm\right) := \rho_*^\pm, \quad \hat{\rho}_k := \hat{\rho}^*, \quad \tilde{\rho}_k := \tilde{\rho}^*, \ \forall k \geq k_0, \tag{18}$$

with $\rho_*^+, \hat{\rho}^*, \tilde{\rho}^* \in \mathbb{R}^+$, $\rho_*^- \in \mathbb{R}^-$. Hence, the switching period error equation (17) boils down to

$$e_k - e_{k-1} = \hat{\rho}^*\left(\Delta_{k-1} - \Delta_k\right) + \rho_*^+\left(\Delta_{k-2} - \Delta_{k-1}\right). \tag{19}$$

The control law proposed for the hysteresis band amplitude in the regulation case is of integral type and answers to the following difference equation:

$$\Delta_k = \Delta_{k-1} + \gamma e_{k-1}, \tag{20}$$

with $\gamma \in \mathbb{R}^+$ denoting the integral constant.

Notice that taking (20) to (19) results in the following linear, homogeneous difference equation with constant coefficients:

$$e_k = \left(1 - \gamma\hat{\rho}^*\right) e_{k-1} - \gamma\rho_*^+ e_{k-2}. \tag{21}$$

Stability of the zero solution of (21), which means $T_k \to T^*$, is studied in next section.

B. The tracking case

Differently from the regulation case, when the system is to track a time-varying reference $x^* = x^*(t)$ the switching function derivatives are not constant even in the steady state regime. As a consequence, the last term of the switching period error equation (17) no longer vanishes, and the sole use of the integral controller (20) yields a linear, non-homogeneous difference equation for the switching period error that does not have $e_k = 0$ as a solution.

Hence, the proposal is to complement the integral action with a feedforward component aiming at compensating the undesirable effect of the previously mentioned term of (17). The SFC structure, shown in Figure 5, consists of setting

$$\Delta_k = \Psi_k + \Omega_k, \tag{22}$$

where Ψ_k is given by an integral control defined as

$$\Psi_k = \Psi_{k-1} + \gamma e_{k-1}, \tag{23}$$

while the feedforward term Ω_k answers to:

$$\Omega_k = \frac{\hat{\rho}_{k-1} - \rho_k^+}{\hat{\rho}_k}\Omega_{k-1} + \frac{\rho_{k-1}^+}{\hat{\rho}_k}\Omega_{k-2} + \frac{\tilde{\rho}_{k-1} - \tilde{\rho}_k}{\hat{\rho}_k}\Psi_{k-1}. \tag{24}$$

Now the switching period error equation matches that of the regulation case, i.e. (21), but with time-varying coefficients:

$$e_k = \left(1 - \gamma\hat{\rho}_k\right) e_{k-1} - \gamma\rho_{k-1}^+ e_{k-2}.$$

Moreover, following Subsection III-A, in the steady-state $x = x^*(t)$ one has that

$$\begin{aligned} \rho_k^\pm &= \rho_k\left(x^*(t), u^\pm\right) := \rho_{*k}^\pm, \\ \hat{\rho}_k &= \hat{\rho}_k\left(x^*(t)\right) := \hat{\rho}_k^*, \\ \tilde{\rho}_k &= \tilde{\rho}_k\left(x^*(t)\right) := \tilde{\rho}_k^*, \end{aligned} \tag{25}$$

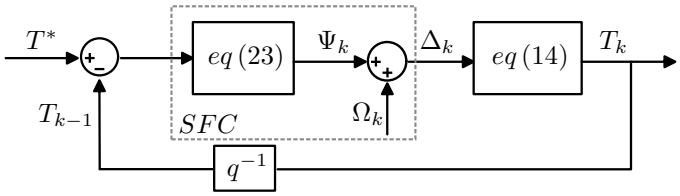

Fig. 5. Switching frequency regulation control loop with feedforward action.

$\forall k \geq k_0$, and the preceding error equation becomes

$$e_k = (1 - \gamma\hat{\rho}_k^*)\, e_{k-1} - \gamma\rho_{*k-1}^{+} e_{k-2}. \tag{26}$$

A stability analysis of the zero solution of (26) is also conducted in next section.

IV. Stability analysis and design criteria

The results obtained in this Section rely upon the hypotheses established in the above analysis. These can be summarized as follows:

Assumption A: The control law (2) induces system (1) to evolve within a boundary layer defined by $|s\,(x, x^*(t))| < \Delta$. Moreover, sliding motion exists on the switching hyperplane $s\,(x, x^*(t)) = 0$ for $\Delta \to 0$, with $x^*(t) \in \mathbb{R}^n$ being the steady state of the ideal sliding dynamics. Finally, $s\,(x, x^*(t))$ shows constant time derivatives at either sides of the switching hyperplane during a complete switching period within the boundary layer.

A. The regulation case

Theorem 1: [1] Let Assumption A be fulfilled, with x^* being a constant regulation point, and let the hysteresis band amplitude, Δ, be updated according to (20). If the integral gain γ is selected as

$$0 < \gamma < \min\left\{\rho_*^{+\,-1}, \left|\rho_*^{-}\right|^{-1}\right\}, \tag{27}$$

with $\rho_*^{\pm}$ defined in (18), then the switching period, T_k, converges asymptotically to its reference value, T^*, in the steady state.

Proof: It follows applying Jury stability criterion to the characteristic polynomial associated to the difference equation (17), see [1] for details. ■

Remark 2: Notice from (20) that as the switching period converges to the desired one, i.e. $e_k \to 0$, then $\Delta_k \to \Delta_{k-1}$, indicating that the hysteresis band amplitude converges to a constant value in the steady state. This fact suggests that the steady state value of the hysteresis band could be obtained from (13); however, this procedure requires knowledge of the switching function derivatives, which are complex to measure due to their high dependence on the system variables and parameters. Instead, the proposed integral control law just demands switching period measures, thus entailing a much simpler implementation procedure.

B. The tracking case

Theorem 2: Let Assumption A be fulfilled, with $x^*(t)$ being a bounded, time-varying tracking reference such that, in the steady state, the absolute value of the switching function derivative inverses, $|\rho\,(x^*(t), u^{\pm})|$, evolve in closed intervals contained in $\mathbb{R}^+$. Let also the real constants γ_m, γ_M defined as

$$\gamma_m := \max\left\{\frac{\hat{\rho}^*(t) - \sqrt{\frac{1}{2}\left(\hat{\rho}^{*^2}(t) - \rho_*^{+^2}(t)\right)}}{\hat{\rho}^{*^2}(t) + \rho_*^{+^2}(t)},\ \forall t \geq 0\right\},$$

$$\gamma_M := \min\left\{\frac{\hat{\rho}^*(t) + \sqrt{\frac{1}{2}\left(\hat{\rho}^{*^2}(t) - \rho_*^{+^2}(t)\right)}}{\hat{\rho}^{*^2}(t) + \rho_*^{+^2}(t)},\ \forall t \geq 0\right\},$$

with $\rho_*^{+}(t), \hat{\rho}^*(t)$ denoting continuous-time functions with sampled counterparts defined in (25), be such that $\gamma_M > \gamma_m$. Finally, let the hysteresis band amplitude, Δ, be updated according to (22). If and the integral gain γ is selected as $\gamma \in (\gamma_m, \gamma_M)$, then the switching period, T_k, converges asymptotically to its reference value, T^*, in the steady state.

Proof: Using the change of variables $y_{1k} = e_{k-1}$, $y_{2k} = e_k$, and defining $y = (y_1, y_2)^\top$, the second-order difference equation (26) can be equivalently written as the first order system

$$y_{k+1} = A_k y_k, \tag{28}$$

with

$$A_k = \begin{pmatrix} 0 & 1 \\ -\gamma\rho_{*k}^{+} & 1 - \gamma\hat{\rho}_{k+1}^* \end{pmatrix} := \begin{pmatrix} 0 & 1 \\ \alpha_k & \beta_{k+1} \end{pmatrix}. \tag{29}$$

Hence, the problem boils down to the stability analysis of the trivial solution $y = 0$ of (28).

Following [32], let us consider the Lyapunov function candidate

$$V_k = y_k^\top Q_k y_k, \quad \text{with} \quad Q_k = \begin{pmatrix} 2\alpha_k^2 + \frac{\delta}{2} & 0 \\ 0 & 1 \end{pmatrix}, \tag{30}$$

$\delta > 0$ being a real constant.

On the one hand, as $\left\{\rho_{*k}^{+}\right\}$ belongs to a closed interval in $\mathbb{R}^+$ by hypothesis, for any $\gamma \in \mathbb{R}$ there exist $\eta_1, \eta_2 \in \mathbb{R}^+$ such that, $\forall k \geq 0$,

$$\eta_1 \mathbb{I}_2 \leq Q_k \leq \eta_2 \mathbb{I}_2, \tag{31}$$

with $\mathbb{I}_2$ standing for the 2×2 identity matrix. On the other hand, the Lyapunov equation

$$A_k^\top Q_{k+1} A_k - Q_k \leq -\eta \mathbb{I}_2,\ \text{with}\ \eta > 0,\ \forall k \geq 0,$$

becomes

$$\begin{pmatrix} \alpha_k^2 + \frac{\delta}{2} - \eta & -\alpha_k\beta_{k+1} \\ -\alpha_k\beta_{k+1} & 1 - 2\alpha_{k+1}^2 - \beta_{k+1}^2 - \frac{\delta}{2} - \eta \end{pmatrix} \geq 0.$$

A Schur complement-based sufficient condition for the preceding matrix to be positive semidefinite is:

$$\alpha_k^2 + \frac{\delta}{2} - \eta > 0 \tag{32}$$

$$\left(\alpha_k^2 + \frac{\delta}{2} - \eta\right)\left(1 - 2\alpha_{k+1}^2 - \beta_{k+1}^2 - \frac{\delta}{2} - \eta\right) \geq \alpha_k^2\beta_{k+1}^2. \tag{33}$$

Recalling again the hypothesis on the evolution of ρ_{*k}^+, the fulfillment of (32) follows selecting $\delta > 2\eta$. In turn, it is sufficient for (33) to be satisfied that

$$\alpha_k^2 + \frac{\delta}{2} - \eta \geq \alpha_k^2, \tag{34}$$

$$1 - 2\alpha_{k+1}^2 - \beta_{k+1}^2 - \frac{\delta}{2} - \eta \geq \beta_{k+1}^2. \tag{35}$$

Notice that $\delta > 2\eta$ also guarantees (34), while for small enough values of δ, η inequality (35) is guaranteed by the demand

$$1 - 2\left(\alpha_{k+1}^2 + \beta_{k+1}^2\right) > 0$$

or, equivalently,

$$\frac{1}{2} > \gamma^2 {\rho_{*k+1}^+}^2 + \left(1 - \gamma\hat{\rho}_{k+1}^*\right)^2.$$

Therefore, γ is to be selected within the interval with bounds given by the roots of the corresponding second-order equation, namely

$$\frac{\hat{\rho}_{k+1}^* \pm \sqrt{\frac{1}{2}\left(\hat{\rho}_{k+1}^{*2} - {\rho_{*k+1}^+}^2\right)}}{\hat{\rho}_{k+1}^{*2} + {\rho_{*k+1}^+}^2}, \quad \forall k \geq k_0. \tag{36}$$

Finally, it follows from Figure 2 and Assumption A that $\rho_{*k}^{\pm}$ can be computed at the same time instant, namely at $t = t_{k-1} + T_k^+$. It is then immediate that the selection of γ within (γ_m, γ_M), which exists by hypothesis, guarantees its belonging to the interval arising from (36), $\forall k \geq k_0$. ■

Remark 3: The definition of $\hat{\rho}$ (see (15)) ensures that γ_m, γ_M are positive real numbers. Its computation can be done off-line using a numerical routine.

Remark 4: The SFC with feedforward action ensures convergence of the switching period error to zero. Therefore, it follows from (23) that the integral part, Ψ_k, converges to a constant value in the steady state. However, as Ω_k is time-varying, the hysteresis band amplitude Δ_k is time-varying as well.

Remark 5: It is worth pointing out that the use of feedforward action in regulation tasks, besides requiring a much complex implementation, has no significant impact on the final result. This can be easily deducted from the fact that, in this case, when taking into account (18), the forced term of (24) is canceled and the corresponding characteristic polynomial has roots in -1 and $-\rho_*^+ (\hat{\rho}^*)^{-1}$, which means that Ω_k converges to the initial condition Ω_0. Therefore,

$$\Delta_k - \Delta_{k-1} \to \Psi_k - \Psi_{k-1} = \gamma e_{k-1},$$

this being the integral control (20) previously used for regulation purposes.

C. Design procedure

The value of γ has to be designed in order to guarantee a stable performance of the switching frequency control loop in all working ranges. The first step requires knowledge of ρ^+ and ρ^- for $x = x^*(t)$, which can be obtained using (10) and (7). The second step consists of obtaining the stability interval for γ, which are given by Theorem 1 in the regulation case and Theorem 2 in the tracking case. As a final step, γ is selected within the corresponding interval and using the following criteria:

i) For the regulation case, one obtains the characteristic polynomial of (21) and chooses a value for γ using pole placement arguments. It is also worth pointing out that when a system is able to operate at different set point values, i.e. x^* can be selected within a certain set $X^* \in \mathbb{R}^n$, the integral gain constant γ should be designed for the worst case. Namely, (27) is to be replaced by

$$0 < \gamma < \min\left\{\frac{1}{\rho\left(x^*, u^+\right)}, \frac{1}{\left|\rho\left(x^*, u^-\right)\right|}, \ \forall x^* \in X^*\right\},$$

in order to guarantee stability at any possible operating point.

ii) For the tracking case it turns out that (26) is time-varying, and pole placement cannot be used. Hence, the suggestion is to choose a conservative value for γ, that is, around the mean value of the stability interval.

V. Numerical simulations

Let us introduce the single-input single-output linear system

$$\dot{x}_1 = -x_1 + x_2, \tag{37}$$

$$\dot{x}_2 = -x_1 + Mu, \tag{38}$$

$M \in \mathbb{R}^+$, which is forced to slide over the switching surface

$$s(x,t) := x_2 - x_2^*(t) = 0, \tag{39}$$

where

$$x_2^*(t) := A + B\sin\omega t, \tag{40}$$

$A, B \in \mathbb{R}$, by the control law (2), with $u^+ = 1$ and $u^- = -1$. Indeed, identifying (37),(38) with (1) one gets that

$$f(x) = \left(-x_1 + x_2, -x_1\right)^\top, \quad g(x) = (0, M)^\top;$$

hence, the equivalent control and the switching function derivative follow immediately from (4) and (5), respectively:

$$u_{eq} = \frac{1}{M}\left(x_1 + \dot{x}_2^*\right), \tag{41}$$

$$\dot{s} = Mu - \left(x_1 + \dot{x}_2^*\right). \tag{42}$$

In accordance with (9), sliding motion exists when

$$M > \left|x_1 + \dot{x}_2^*\right|,$$

with the ideal sliding dynamics given by

$$x_2 = x_2^*(t), \tag{43}$$

$$\dot{x}_1 = -x_1 + x_2^*(t). \tag{44}$$

Notice that the steady state solution of (44), which answers to

$$x_1^*(t) = A + \frac{B}{1+\omega^2}\left(\sin\omega t - \omega\cos\omega t\right), \tag{45}$$

is asymptotically stable. Once the ideal steady state sliding regime $x^* = (x_1^*, x_2^*)^\top$ has been reached, the switching function derivative inverses at either sides of the switching hyperplane, computed using (42), (45) and (40), are

$$\rho_*^{\pm}(t) = \left(\pm M - A - \frac{B}{1+\omega^2}\left(\sin\omega t - \omega^3\cos\omega t\right)\right)^{-1}. \tag{46}$$

for the tracking case, and

$$\rho_*^{\pm} = \frac{1}{\pm M - A} \tag{47}$$

for the regulation case.

Simulation results for system (37),(38) in both regulation and tracking situations are reported next. They have been performed with Matlab-Simulink using the following parameters: $M = 3$, $A = 1$, and $\omega = 2\pi \cdot 0.02$, while the switching period reference has been set to $T^* = 0.1s$.

A. The regulation case

In this case $B = 0$ and, consequently, $x^* = (1, 1)^\top$. In turn, it stems from (47) that $\rho_*^+ = 0.5$ and $\rho_*^- = -0.25$. Hence, following Theorem 1 and inequality (27), under the SFC with control law given in (20) the closed-loop system is stable for $0 < \gamma < 2$.

Figure 6 shows the response of the SFC for different values of γ and T^*.

The evolution of the switching function, s, is depicted at the bottom part of the figures. The mid part contains the switching period of the system (37),(38), i.e. T_k, as well as the switching period arising from the solution of the system of difference equations (20),(21), which is labeled as T_k^m. The plot illustrates how Δ_k is updated until T_k attains the reference value T^*, with shorter transients for higher values of γ. In turn, during the start-up, where the steady state sliding motion is still not reached, T_k^m does not match T_k due to the fact that $\rho^{\pm} \neq \rho_*^{\pm}$. Once the system attains the sliding mode steady state, i.e. $\rho^{\pm} = \rho_*^{\pm}$, both responses match perfectly, even under a switching period reference variation occurring at $t = 12s$; this provides additional evidence of the validity of the mathematical model of the switching frequency behavior presented in Sections II and the assumptions made in Section III-A. Finally, it is worth emphasizing that the hysteresis band amplitude attains a constant value in the steady state, as pointed out in Remark 2. The asymptotic tendency of the state variables to the reference is illustrated in the upper part of the figure through the behavior of x_1.

B. The tracking case

The selected amplitude of the reference signal is now $B = 0.5$. With these settings it is immediate from (46) that $\rho_*^{\pm}(t)$ are bounded; therefore, the functions $\rho_+^*(t)$ and $\hat{\rho}^*(t)$, used to obtain an interval for the control gain where stability is guaranteed, are bounded as well. Hence, following Theorem 2, under the SFC with the control law given in (22) uniform exponential stability of the closed-loop system is ensured for $0.314 < \gamma < 1.0315$.

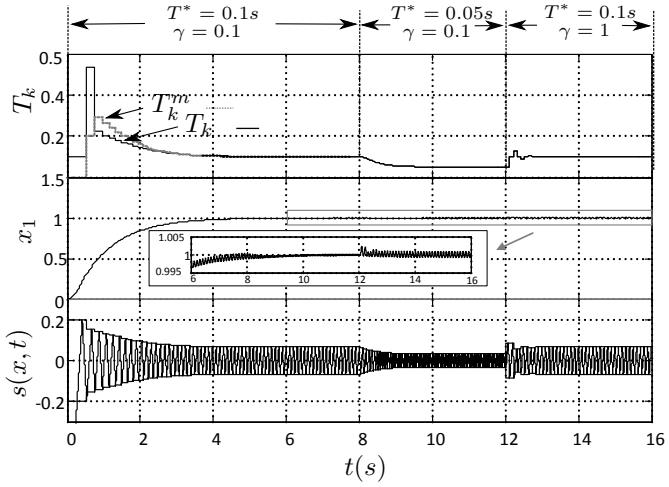

Fig. 6. Regulation: performance of the SFC for different values of γ and T^*.

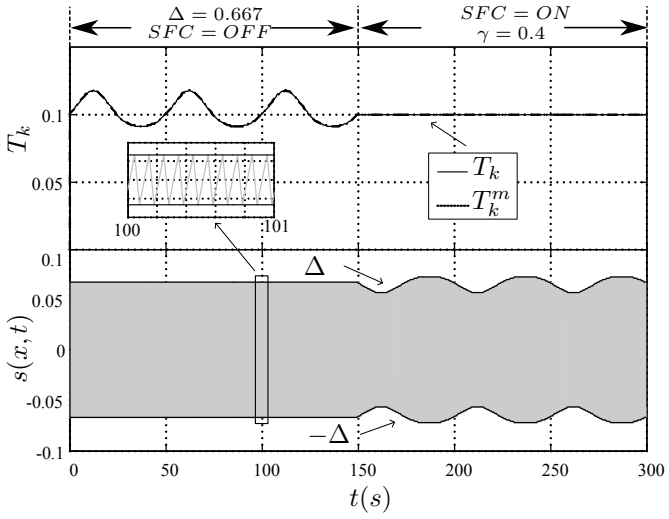

Fig. 7. Tracking: evolution of T_k and s with fixed hysteresis for $t < 150s$ and SFC for $t \geq 150s$.

It is worth remarking that numerical simulations show that stability is indeed guaranteed for $0 < \gamma < 1.6$. The conservativeness of the interval steming from the theoretical analysis is due to the sufficiency of the obtained condition.

Figure 7 compares the performance of the system without and with SFC action. The SMC operates with fixed hysteresis band for the first $t = 150s$, an then the SFC with $\gamma = 0.4$ is enabled: notice that it is not until the activation of the SFC (22) that T_k is able to attain the reference value $T^* = 0.1s$. Figure 8 shows that the SFC is also able to cope with a change of T^*. Finally, Figure 9 presents the dynamics of x_2, T_k and s for changes in frequency and amplitude of the reference signal $x_2^*(t)$: good behavior of the state and proper regulation

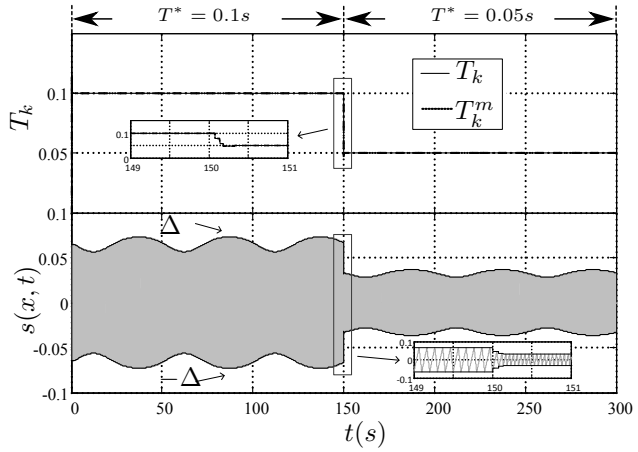

Fig. 8. Tracking: evolution of T_k and s when T^* is changed from $0.1s$ to $0.05s$.

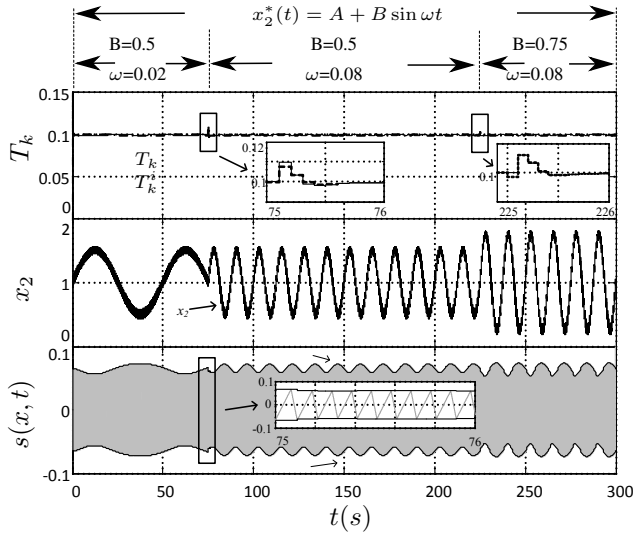

Fig. 9. Tracking: evolution of T_k, x_2 and s when the frequency and amplitude of $x_2^*(t)$ are changed from $\omega = 0.02$ to $\omega = 0.08$ and from $B = 0.5$ to $B = 0.75$, respectively.

of the switching period validate the proposal. Similar results are obtained for changes in the offset of x_2^*, again omitted for the sake of brevity. Finally, the time variation of Δ_k required to keep a constant switching period in tracking tasks pointed out in Remark 4 can be observed in Figures 7-9.

Figures 7-9 also incorporate the switching period T_k^m, now obtained solving (22)-(26). As happened in the regulation case the differences with T_k arise only in sliding mode transients, which again confirms the validity of models and assumptions of Sections II and III-B.

VI. Experimental results

The proposed control laws have been tested in the step-down switching power converter shown in Figure 10. Its dynamics are governed by:

$$C\frac{dv_C}{dt} = -\frac{v_C}{R} + i_L, \tag{48}$$

$$L\frac{di_L}{dt} = -v_C + Eu, \tag{49}$$

where i_L is the inductor current, v_C is the output voltage, R is the resistive load, L is the inductance, C is the capacitor and E is the input voltage. In turn, the output voltage reference is selected as

$$v_C^*(t) = v_{C0} + v_{C1}\sin\omega t. \tag{50}$$

Table I shows the specific values of the converter parameters used in the experimentation. The control signal u drives the power switches states -MOSFETs PSMN013R100BS from NXP in this case- and takes discrete values, namely, $u \in \{0, 1\}$. The employed MOSFETs driver is LM5106 from Texas Instruments. It is also remarked that the dead time is of 0.1 μs.

Since the relative degree of the output voltage with respect to the control is two, the following first order, linear switching surface is used to tame the output voltage [2], [5] :

$$s\left(v_C, \dot{v}_C\right) = \lambda_1\left(v_C - v_C^*\right) + \lambda_2 C\left(\dot{v}_C - \dot{v}_C^*\right) = 0, \quad \lambda_{1,2} > 0. \tag{51}$$

As $\lambda_2 E > 0$, the control law (2) with $u^+ = 1$ and $u^- = 0$ forces sliding motion over $s = 0$. Identifying (48),(49) with (1), the equivalent control and the switching function derivative can be easily obtained from (4) and (5), respectively:

$$u_{eq} = \frac{1}{E}\left(-\frac{\alpha\lambda_1}{\lambda_2}i_L + \left(1 + \frac{\alpha\lambda_1}{R\lambda_2}\right)v_C\right) + \frac{L}{E}h(t), \tag{52}$$

$$\dot{s} = \frac{E\lambda_2}{L}\left(u - u_{eq}\right). \tag{53}$$

with

$$\alpha := \frac{L}{C}\left(1 - \frac{\lambda_2}{R\lambda_1}\right) \quad \text{and} \quad h(t) := \frac{\lambda_1}{\lambda_2}\dot{v}_C^* + C\ddot{v}_C^*.$$

As $E\lambda_2 > 0$, the control law (2) with $u^+ = 1$ and $u^- = 0$ forces sliding motion over $s = 0$. The corresponding ideal sliding behavior when $\Delta \to 0$ is given by the linear, time-

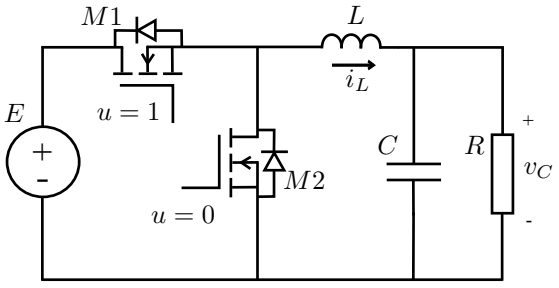

Fig. 10. Step-down switching power converter.

TABLE I. POWER CONVERTER PARAMETERS.

E	$48V$
L / C	$22\mu H$ / $50\mu F$
Output load (R)	$2\Omega - 4\Omega - 8\Omega$
Output voltage offset (v_{C0})	$12V - 24V$
Output voltage amplitude (v_{C1})	$0V - 12V$
Output voltage frequency (f)	$100Hz - 800Hz$
Output current	$0A - 6A$
Switching period reference (T^*)	$10\mu s$
MOSFETS (M1,M2)	$PSMN013100BS$
MOSFET Driver	$LM5106$
Dead Time	$0.1\mu s$

varying system:

$$C\frac{dv_C}{dt} = -\frac{\lambda_1}{\lambda_2}v_C + \frac{\lambda_1}{\lambda_2}v_C^* + C\dot{v}_C^*,$$
$$L\frac{di_L}{dt} = \frac{\alpha\lambda_1}{R\lambda_2}v_C - \frac{\alpha\lambda_1}{\lambda_2}i_L + Lh(t),$$

It is then immediate that the steady-state solution is asymptotically stable if and only if

$$0 < \frac{\lambda_2}{\lambda_1} < R. \tag{54}$$

The switching function derivative inverses at either sides of the boundary layer when the ideal steady state sliding regime is reached answer to:

$$\rho_*^{\pm}(t) = \lambda_2^{-1}\left(\frac{Eu^{\pm}}{L} - \frac{v_C^*}{L} - \frac{\dot{v}_C^*}{R} - C\ddot{v}_C^*\right)^{-1} =$$
$$= \lambda_2^{-1}\left(\frac{Eu^{\pm} - v_{C0}^*}{L} - D\sin(\omega t + \phi)\right)^{-1}, \tag{55}$$

with

$$D := v_{C1}\sqrt{\left(\frac{\omega}{R}\right)^2 + \left(\frac{1}{L} - C\omega^2\right)^2},$$
$$\phi := \arctan\frac{L\omega}{R(1 - LC\omega^2)}.$$

The implementation of the switching surface and the hysteresis comparator has been carried out with analog electronics, whereas the switching period measure and the tuning of the values of the hysteresis band amplitude have been performed with the digital processor STM32F047, which is a microcontroller with two digital-to-analog converters used to adapt the hysteresis values. The switching surface parameters have been set to $\lambda_1 = 0.2$, $\lambda_2 = 0.38$, which provides sliding mode transient response of the desired output voltage with a time constant of 95 μs.

It is also important for a good performance of the SFC that the computing delay, i.e. the time, t_c, taken by the micro controller to calculate the next value of Δ, is lower than T^+, as depicted in Figure 12. When this condition is not fulfilled, the switching period model (14) is no longer valid. In our case we have that $t_c = 1.4\mu s$, while the highest value of T^+ is $2.5\mu s$.

A. DC output voltage regulation

In this case $v_{C1} = 0$ and, consequently, $v_C^* = v_{C0}$. The inverse of the switching function derivatives in the steady state, obtained from (55), are given by $\rho_*^+ = \lambda_2 L^{-1}(E - v_C^*)$ and $\rho_*^- = -\lambda_2 L^{-1} v_C^*$. According to Table I we now have two voltage references, namely $v_C^* = 12V$ and $v_C^* = 24V$. Hence, following Theorem 1 and Subsection IV-C the admissible values of the integral gain γ of the SFC (20) to ensure closed-loop stability have to be selected as $\gamma \in (0, 207272)$, as the worst case arises with $v_C^* = 12V$; this parameter is initially set to $\gamma = 20000$. It has to be pointed out that the control implementation is simple, since it just requires measuring the switching period and performing the difference equation (20).

The following oscilloscope captures illustrate the behavior of the output voltage (blue waveform), the switching function (green waveform), the upper hysteresis of the comparator (magenta waveform), and the switching period (red waveform); the latter appears converted to voltage with a rate of $3.5V/10\mu s$. As the comparator MC6567 is supplied between 0 and $5V$, the offset value of the switching function is set at $2.5V$ in order allow a symmetrical use of the full input range.

Figures 13 and 14 present the start-up of the converter when the output voltage is regulated to $12V$ for different initial conditions of the hysteresis band amplitude Δ_0, namely, lower and higher than the steady state value, respectively. Notice that both v_C and T_k attain their references with a good transient response, while the hysteresis band is adapting till T_k reaches T^*. Notice that T_k can be easily measured looking at the switching function in the zoomed window. As observed in Remark 2, once T_k stabilizes the hysteresis band Δ_k remains constant. The output load value selected in this case is $R = 2\Omega$, with which (54) is fulfilled.

Figure 15 shows again good performance for a voltage regulation from 12 to 24V and vice-versa, with $R = 4\Omega$. In this case the jumps of v_C^* and, consequently, the change of switching function drops the hysteresis amplitude value and recovers it again in less than one switching period, this entailing a brief, smooth transient of T_k.

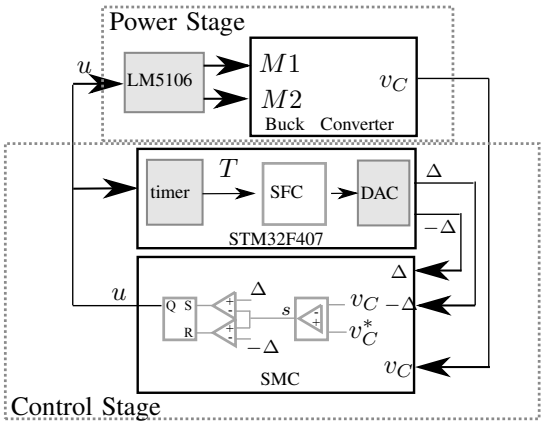

Fig. 11. Implementation details: the SMC with a variable hysteresis comparator is implemented using analogue circuitry, while the SFC is implemented using a DSP STM32F407.

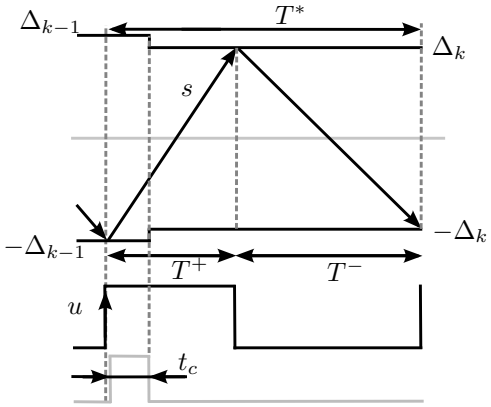

Fig. 12. Effect of the computing delay related to DSP microcontroller.

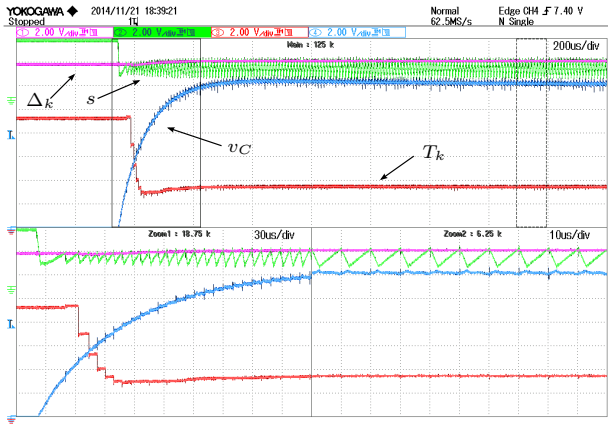

Fig. 13. Regulation: start-up for $v_C^* = 12V$ with $R = 2\Omega$ and Δ_0 lower than the steady state value. v_C: blue; s: green; $|\Delta_k|$: magenta; T_k: red.

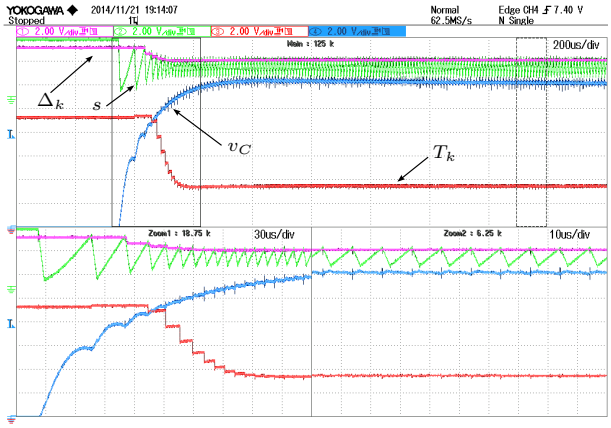

Fig. 14. Regulation: start-up for $v_C^* = 12V$ with $R = 2\Omega$ and Δ_0 higher than the steady state value. v_C: blue; s: green; $|\Delta_k|$: magenta; T_k: red.

Finally, in Figure 16 the integral gain is set to $\gamma = 200000$, while R is kept at 4Ω and T^* is varied from $12.5\mu s$ to $14\mu s$.

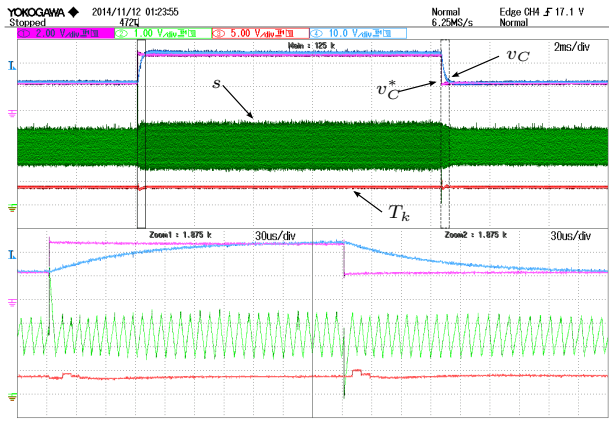

Fig. 15. Regulation: v_C^* variation from $12V$ to $24V$ and vice-versa, with $R = 4\Omega$. v_C: blue; s: green; v_C^*: magenta; T_k: red.

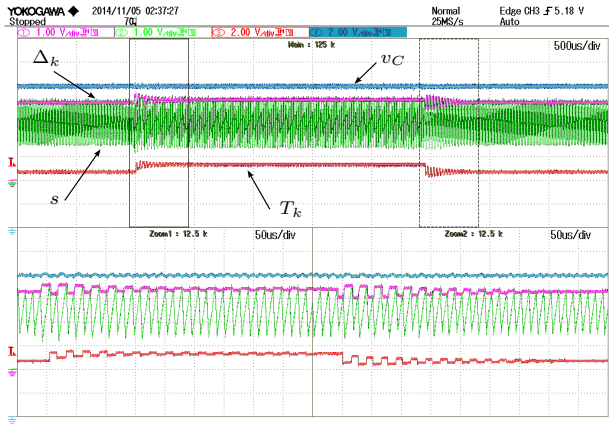

Fig. 16. Regulation: underdamped responses for $\gamma = 200000$ with $R = 4\Omega$ and a T^* variation from $12.5\mu s$ $14\mu s$. v_C: blue; s: green; $|\Delta_k|$: magenta; T_k: red.

As γ is now closer to the upper stability limit, both T_k and Δ_k exhibit underdamped transient responses with very low damping ratio, thus confirming the theoretical prediction.

B. AC output voltage tracking

As indicated in Table I, the offset and amplitude of the output voltage profile are $v_{C0} = 24V$ and $v_{C1} = 12V$, respectively, while $R = 8\Omega$. Thus, it follows from (55) that $\rho_*^{\pm}(t)$ are bounded, and so is $\hat{\rho}^*(t)$. Hence, it stems from Theorem 2 that the SFC with control law given in (22) yields a uniformly exponentially stable closed-loop system for $43383 < \gamma < 143170$. Nevertheless, as it happened with the numerical example, the closed-loop system is still stable for positive values lower than 42142. Taking into account the stability range the integral gain has been set to $\gamma = 75000$.

It has to be remarked that the SFC implementation for the tracking case is not as simple as it was for the regulation case.

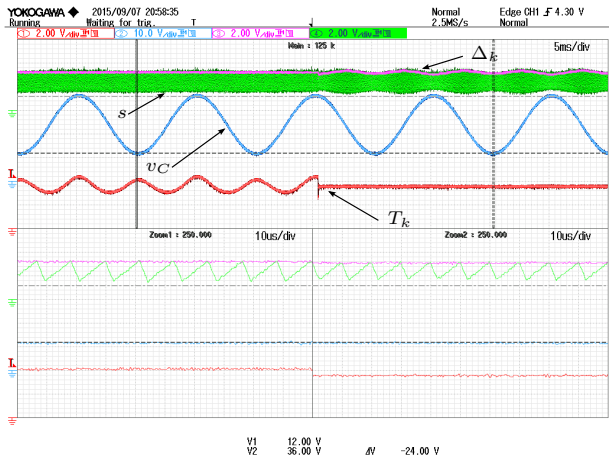

Fig. 17. Tracking: system perfomance without and with SFC. v_C: blue; s: green; $|\Delta_k|$: magenta; T_k: red.

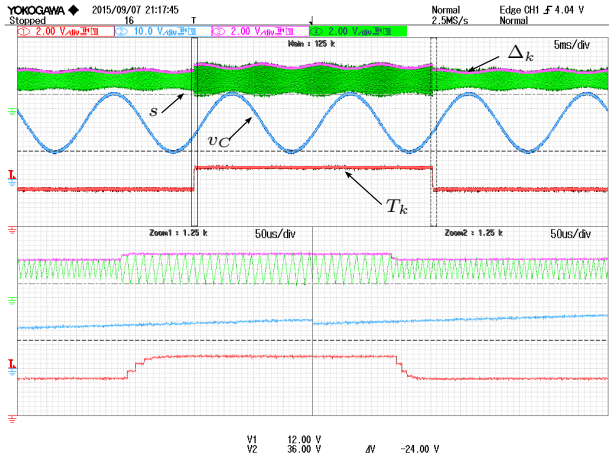

Fig. 18. Tracking: T^* variation from $9\mu s$ to $14\mu s$. v_C: blue; s: green; $|\Delta_k|$: magenta; T_k: red.

This is because the SFC control (22) includes the feedforward term Ω_k introduced in (24), which requires knowledge of the current switching function derivatives, i.e. at period k. Of course the hysteresis band amplitude Δ_k should be calculated at the beginning of the period, when the available information is that of the $k-1$ switching period. Therefore, the implemented value of Ω_k is approximated by Ω_{k-1}, and the values of the switching function derivatives are calculated as

$$\rho^+_{k-1} = \frac{T^+_{k-1}}{\Delta_{k-1}+\Delta_{k-2}}, \quad \rho^-_{k-1} = \frac{T^-_{k-1}}{2\Delta_{k-1}},$$

in accordance with Figure 2.

In the first test the system operates with fixed hysteresis amplitude until the SFC is enabled. Figure 17 shows the switching period rapidly reaching the reference value $T^* = 10\mu s$ after the activation of the SFC, together with an overall good performance of the system.

The second test gives evidence of the performance of SFC

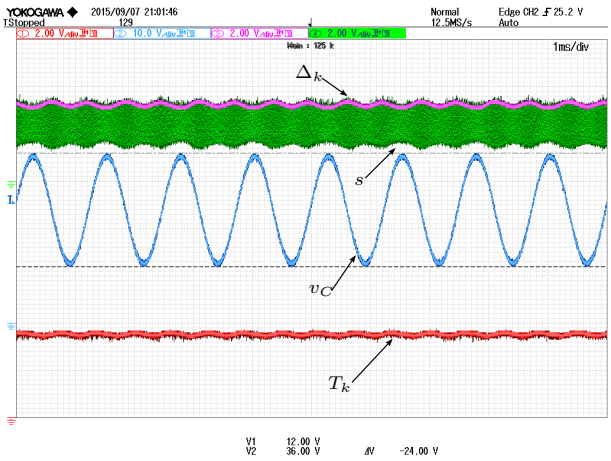

Fig. 19. Tracking: system response when the frequency of the sinusoidal output voltage reference is set to $800Hz$. v_C: blue; s: green; $|\Delta_k|$: magenta; T_k: red.

under changes of the switching period reference, specifically from $T^* = 9\mu s$ to $T^* = 14\mu s$. As illustrated in Figure 18, the switching period presents an overdamped response and only three or four switching periods are required for the hysteresis values to properly adapt and force the switching frequency to attain the new reference. Notice that a time-varying hysteresis amplitude is required to keep a constant steady state switching period, as indicated in Remark 4 and already observed in Figure 17.

In the last test the frequency of the voltage reference v_C^* is set to $800Hz$. The corresponding range of the integral gain of the SFC ensuring uniform exponential stability becomes $43251 < \gamma < 143020$. It can be seen in Figure 19 that now the switching frequency is not perfectly regulated, and a very small variation around T^* arises. This is because, on the one hand, the error associated to the compromise solution adopted to solve the above indicated computational issue with the feedforward signal Ω_k is significant for high frequency voltage references; and, on the other hand, these high frequencies also invalidate the assumption of piecewise linear behavior of the switching function within one switching period, thus entailing inaccuracy of the mathematical model. Nevertheless, although a perfect regulation is not achieved the result is still good enough for most applications.

VII. Conclusions

An SFC was proposed for SMC applications that use a hysteresis band comparator. By modifying the amplitude of the hysteresis band, the controller provides fixed steady state switching frequency under standard assumptions. For regulation purposes the proposed SFC is of integral type, while the inclusion of an additional feedforward term allows its use also for tracking tasks. A mathematical model of the switching frequency behavior for time-varying hysteresis band amplitudes was crucial to devise the controllers and to carry out subsequent stability analyses. Simulation and experimental results showed an excellent performance of the controllers,

as well as their robustness to changes in the switching frequency reference and system parameters. The method can be extended to other advanced sliding mode controllers and even to hysteretic controllers when the aforementioned hypotheses are fulfilled.

The entire work lies on the assumption of piecewise linear behavior of $s(x,t)$ inside the boundary layer. Further research should investigate the possibility of relaxing this hypothesis to work not with constant values but just with bounds of $\dot{s}^{\pm}$ within one switching period.

REFERENCES

[1] V. Repecho, D. Biel, and E. Fossas, "Fixed switching frequency sliding mode control using a hysteresis band controller", *Proc. 13th Internat. Workshop on Variable Structure Systems (VSS)*, 2014.

[2] F. Bilalović, O. Musić, and A. Sabanović, "Buck converter regulator operating in the sliding mode", *Proc. VII International PCI*, 1983, pp. 331–340.

[3] R. Venkataramanan, *Sliding mode control of power converters*, PhD Thesis, California Institute of Technology, Pasadena, California, 1986.

[4] H. Bühler, *Réglage par mode de glissement*, Presses Polytechniques Romandes, 1986.

[5] M. Carpita and M. Marchesoni,"Experimental study of a power conditioning system using sliding mode control", *IEEE Trans. Power Electronics*, Vol. 11, pp. 731–742 (1996).

[6] T. Siew-Chong, Y. M. Lai, M. K. H. Cheung, and C.K. Tse, "On the practical design of a sliding mode voltage controlled buck converter", *IEEE Trans. Power Electronics*, Vol. 20, pp. 425–437 (2005).

[7] J. Korelic and K. Jezernik, "Predictive variable-structure system control of unity power factor rectifiers", *IET Power Electronics*, Vol. 6, pp. 1608–1617 (2013).

[8] H. Komurcugil, "Double-band hysteresis current-controlled single-phase shunt active filter for switching frequency mitigation", *Electrical Power and Energy Systems*, Vol. 69, pp. 131–140 (2015).

[9] H. Komurcugil, S. Ozdemir, I. Sefa, N. Altin, and O. Kukrer, "Sliding-mode control for single-phase grid-connected LCL-filtered VSI with double-band hysteresis scheme", *IEEE Trans. Industrial Electronics*, Vol. 63, pp. 864–873 (2016).

[10] J.M. Ruiz, S. Lorenzo, I. Lobo, and J. Amigo, "Minimal UPS structure with sliding mode control and adaptive hysteresis band", *Proc. 16th IEEE Industrial Electronics Society Conf. (IECON)*, 1990, Vol. 2, pp. 1063–1067.

[11] C. Chiarelli, L. Malesani, S. Pirondini, and P. Tomasin, "Single-phase, three level, constant frequency current reference hysteresis control for UPS applications", *Proc. European Power Electronics Conf. (EPE)*, 1993, pp. 180–185.

[12] L. Malesani, L. Rossetto, G. Spiazzi, and P. Tenti, "Sliding mode control of SEPIC converters", *Proc. European Space Power Conference (ESPC)*, 1993, pp. 173–178.

[13] L. Malesani, L. Rossetto, G. Spiazzi, and A. Zuccato, "An AC power supply with sliding-mode control", *IEEE Industry Applications Magazine*, Vol. 2, pp. 32–38 (1996).

[14] D.G. Holmes, R. Davoodnezhad, and B.P. McGrath, "An improved three-phase variable-band hysteresis current regulator", *IEEE Trans. Power Electronics*, Vol. 31, pp. 758–769 (2013).

[15] R. Guzman, L. Garcia de Vicuña, J. Morales, M. Castilla, and J. Matas, "Sliding-mode control for a three-phase unity power factor rectifier operating at fixed switching frequency," *IEEE Trans. Power Electronics*, Vol. 31, pp. 758–769 (2016).

[16] J. F. Silva and S. S. Paulo, "Fixed frequency sliding mode modulator for current mode PWM inverters", *Proc. 24th IEEE Power Electronics Specialists Conf. (PESC)*, 1993, pp. 623–629.

[17] P. Mattavelli, L. Rossetto, G. Spiazzi, and P. Tenti, "General-purpose sliding-mode controller for DC/DC converter applications", *Proc. 24th IEEE Power Electronics Specialists Conf. (PESC)*, 1993, pp. 609–615.

[18] E. Fossas, R. Griñó, and D. Biel, "Quasi-Sliding control based on pulse width modulation, zero averaged dynamics and the L_2 norm", *World Scientific*, pp. 335–344, 2001.

[19] R. Ramos, D. Biel, E. Fossas, and F. Guinjoan, "A fixed-frequency quasi-sliding control algorithm: application to power inverters design by means of FPGA implementation", *IEEE Trans. Power Electronics*, Vol. 18, pp. 344-355 (2003).

[20] J. Mahdavi, A. Emadi, and H.A. Toliyat, "Application of state space averaging method to sliding mode control of PWM DC/DC converters", *Proc. 32nd Industry Applications Conf. (IAS)*, 1997, Vol. 2, pp. 820–827.

[21] T. Siew-Chong, Y.M. Lai, C.K. Tse, and M.K.H. Cheung, "A fixed-frequency pulsewidth modulation based quasi-sliding-mode controller for buck converters", *IEEE Trans. Power Electronics*, Vol. 20, pp. 1379–1392 (2005).

[22] T. Siew-Chong, Y.M. Lai, and C.K. Tse, "General Design Issues of Sliding-Mode Controllers in DC-DC Converters", *IEEE Trans. Industrial Electronics*, Vol. 55, pp. 1160–1174 (2008).

[23] M. Teodorescu and D. Stanciu, "Sliding coefficients estimation for fixed frequency sliding mode control of boost converter", *Proc. 9th Internat. Symp. on Advanced Topics in Electrical Engineering (ATEE)*, 2015, pp. 698–703.

[24] S. C. Huerta, P. Alou, J.A. Oliver, O. García, J.A. Cobos, and A. Abou-Alfotouh, "Nonlinear control for DC-DC converters based on hysteresis of the C_{OUT} current with a frequency loop to operate at constant frequency", *IEEE Trans. Industrial Electronics*, Vol. 58, pp. 1036-1043 (2011).

[25] J. Ye, P. Malysz and A. Emadi, "A fixed-switching-frequency integral sliding mode current controller for switched reluctance motor drives", *IEEE J. Emerging and Selected Topics in Power Electronics*, Vol. 3, pp. 698–703 (2015).

[26] A. Abrishamifar, A.A. Ahmad, and M. Mohamadian, "Fixed switching frequency sliding mode control for single-phase unipolar inverters", *IEEE Trans. Power Electronics*, Vol. 27, pp. 2507–2514 (2012).

[27] S. C. Huerta, P. Alou, J.A. Oliver, O. García, J.A. Oliver, R. Prieto, and J.A. Cobos, "Hysteretic Mixed-Signal Controller for High-Frequency DCDC Converters Operating at Constant Switching Frequency", *IEEE Trans. Power Electronics*, Vol. 27, pp. 2690-2696 (2012).

[28] W.T. Yan, C.N.M. Ho, H.S.H. Chung, and K.T.K. Au, "Fixed-Frequency Boundary Control of Buck Converter With Second-Order Switching Surface", *IEEE Trans. Power Electronics*, Vol. 24, pp. 2193–2201 (2009).

[29] L. Malesani, P. Mattavelli, and P. Tomasin, "Improved Constant-Frequency Hysteresis Current Control of VSI Inverters with Simple Feedforward Bandwidth Prediction", *IEEE Trans. Industry Applications*, Vol. 33, pp. 1194-1202 (1997).

[30] V. Utkin, J. Guldner, and J. Shi, *Sliding Mode Control in Electromechanical Systems*, CRC Press, 1999.

[31] H. Sira-Ramírez, "Differential geometric methods in variable structure control", *Internat. J. Control*, Vol. 48, pp. 1359–1390 (1988).

[32] W.J. Rugh, *Linear Systems Theory*, Prentice Hall, 1996.

ACKNOWLEDGEMENTS

The authors are partially supported by the spanish projects DPI2013-41224-P (Ministerio de Educación) and 2014 SGR 267 (AGAUR).

Víctor Repecho (Barcelona, Spain, 1984) received the B.S and M.S. degrees in electronic engineering from the Universitat Politècnica de Catalunya (UPC), Barcelona, Spain, in 2006 and 2012, respectively. Since 2010, he has been a development Engineer with the Institute of Industrial and Control Engineering (IOC), UPC. His research fields are related to digital control, nonlinear control, and control of power electronic converters.

Domingo Biel () received the B.S, M.S. and Ph.D. degrees in telecommunications engineering from the Universitat Politècnica de Catalunya (UPC), Barcelona, Spain, in 1990, 1994 and 1999, respectively. Since 1998, he has been an Associate Professor in the Electronic Engineering Department, UPC, where he teaches power electronics and control theory. He is the coauthor of around 20 papers in international journals and more than 50 communications in international conferences. His research fields are related to nonlinear control and its application to renewable energy systems and power electronics.

Josep M. Olm (Mataró, Spain, 1966) received the M.S. and Ph.D. degrees in Physics from the Universitat de Barcelona and the Universitat Politècnica de Catalunya (UPC), both in Barcelona, Spain, in 1989 and 2004, respectively. Since 2003 he is with UPC, where he is currently an Associate Professor at the Department of Mathematics and the Institute of Industrial and Control Engineering.

His research interests are in the field of control theory, including sliding, adaptive, repetitive, and complex networks control. He is author or co-author of more than 50 journal articles and conference papers.

Dr. Olm is Member of the IEEE Circuits and Systems Society, and served as Associate Editor of the IEEE Transactions on Circuits and Systems-I: Regular Papers during the term 2014-2015.

Enric Fossas Colet (Aiguafreda, 1959) graduated in Mathematics in 1981 and received the Ph.D. degree in Mathematics in 1986, both from Universitat de Barcelona. In 1986 he joined the Department of Applied Mathematics, Universitat Politecnica de Catalunya, where he served as Head of Department from 1993 to 1999. In 1999 he moved to the Department of Automatic Control and Computer Engineering and to the Institute of Industrial and Control Engineering, being the director of the Institute from July, 2003 to July, 2009. He is full professor in Control Systems and Automation. In December 2013 he was appointed Rector of the Universitat Politècnica de Catalunya.

His research interests includes nonlinear control (theory and applications), particularly Variable Structure and Hybrid Systems, with applications to switching converters. He is author/co-author of more than 100 scientific papers presented in conferences or published in specialized journals. He is co-author of four books: Nonlinear Dynamics in Power Electronics (IEEE), Variable Structure Systems and Applications (IEE, LNCS) and Port-Controlled Hamiltonian Systems (LNCS). He is member of the UPC research group "Advanced Control on Energy Systems".